IEEE Access
Multidisciplinary | Rapid Review | Open Access Journal

Received September 26, 2019, accepted October 15, 2019, date of publication October 18, 2019, date of current version October 30, 2019.

Digital Object Identifier 10.1109/ACCESS.2019.2948191

Dielectrophoretic Microfluidic Chip Integrated With Liquid Metal Electrode for Red Blood Cell Stretching Manipulation

BOTAO ZHU[1], YIFAN CAI[1], ZHENGTIAN WU[2], FUZHOU NIU[2], AND HAO YANG[1], (Member, IEEE)

[1]Robotics and Microsystems Center, School of Mechanical and Electric Engineering, Soochow University, Suzhou 215000, China
[2]Suzhou University of Science and Technology, Suzhou 215009, China

Corresponding author: Hao Yang (yhao@suda.edu.cn)

This work was support in part by the National Natural Science Foundation of China under Grant 61703294, in part by the Natural Science Foundation of Jiangsu Province under Grant BK20170342, in part by the Natural Science Foundation of the Jiangsu Higher Education Institutions of China under Grant 18KJB460026, and in part by the China Postdoctoral Science Foundation under Grant 2017M611897.

ABSTRACT Cellular mechanical properties are closely related to cell physiological functions and status, and their analysis and measurement help understand cell mechanism. In this study, a microfluidic platform was built to measure the mechanical properties of cells by using dielectrophoretic (DEP) force. The electrodes generally used to stretch cells are made of indium tin oxide, Au, and Pt, which have inherent disadvantages. In this paper, galinstan alloy liquid metal was first introduced as microelectrode to form non-uniform electric filed for red blood cell stretching manipulation. The liquid metal microelectrode is easy to manufacture, low in price, stable at high voltage, and reusable. An effective microfluidic chip integrated with liquid metal electrode was designed and simulated, and a series of experiments to capture and stretch red blood cells was performed. The length of the red blood cells increased from 6 μm to 8 μm under the DEP force from 0 pN to 103 pN. This work also revealed the potential use of liquid metal as microelectrode to manipulate the microparticles and cells in a microfluidic chip.

INDEX TERMS Liquid metal electrode, galinstan, dielectrophoresis, microfluidic chip, cell stretching.

I. INTRODUCTION

Cells are the basic unit of life. The in-depth study of biological cell is the key to uncover physiological processes and cure diseases [1], [2], [32]. Cellular properties have been studied using a series of techniques via effective cell manipulation, which mainly includes cell rotation, separation, transportation, injection, and stretching [4]–[9]. Biological processes, such as cell growth, differentiation, division, and apoptosis in life, are directly affected by the mechanical properties of the cell [10], [11]. Cellular physiological function deterioration leads to abnormalities in cell mechanical properties and eventually various diseases [12]–[14]. Cell stretching is one of the most important tasks in cell manipulation and can obtain the mechanical properties of cells. The mechanical properties of cells directly affect their cell morphology and structure and thereby dominate their biological functions [15], [16].

The associate editor coordinating the review of this manuscript and approving it for publication was Sanket Goel.

The methods for evaluating the cell mechanical properties can be divided into contact and noncontact techniques. Contact measurement, such as micropipette suction, microinjection, and atomic force microscopy, stretches or compresses the cell through mechanical contact [17]–[22]. However, physical contact with the measurement equipment may damage the cells during the experiment. Non-contact techniques, such as optical tweezers, magnetic twisting cytometry, and dielectrophoresis (DEP) were introduced subsequently to precisely determine the mechanical properties without physical damage [10], [23]–[28]. However, harmful heat is produced from the long-term use of high-energy lasers to manipulate cells. The cells must be magnetized with magnetic beads coated with proteins prior to manipulation. DEP has attracted increasing attention in measuring the mechanical properties of cells because of its advantages such as no label, low cost, high flux, and minimal damage [29]–[31]. The materials generally used to form microelectrode include indium tin oxide (ITO), Au, and Pt.

However, stretching different cells requires electrodes of different spacing levels, thus increasing the cost and necessitating cumbersome processes. Therefore, a new type of material that can be used to conveniently manufacture microelectrode is highly needed.

Galinstan liquid metal has been used in various macroscopic and microscopic applications, such as liquid metal motors [32], liquid metal driven microfluidic pumps, and variable liquid metal circuits [33], [34] due to its special advantages. However, this material has not been introduced into microfluidics chip as a microelectrode. The use of Galinstan liquid metal as an electrode in a microchannel is feasible because of its excellent electrical conductivity and large surface tension [35]–[37].

This study built a cell manipulation system, which mainly includes a microscope, a voltage signal generator, two microfluidic pumps and a microfluidic chip, that measures and analyzes the mechanical properties of red blood cells. A novel microfluidic chip containing a pair of electrodes made of liquid metal and ITO was designed and fabricated. Galinstan liquid metal was introduced as a microelectrode to form non-uniform electric field. The use of a liquid metal electrode enables the fast and accurate measurement of the mechanical properties of cells without extremely complicated microfluidic chip fabrication. The thickness of the ITO electrode was 180 nm, whereas that of the liquid metal electrode was 50 μm. The height difference between the liquid metal and ITO electrodes generated a sufficient electric field gradient to stretch the cells. We innovatively stretched biological cells using the electrode formed by liquid metal. A series of experiments was performed to stretch mouse red blood cells using liquid metal and ITO electrodes and analyze their mechanical properties. The experimental results were compared with several previous works to reveal the accuracy of the proposed method [38]–[41]. The proposed cell stretching method also provided a new approach to study cell mechanism in single cell level, thereby contributing to the treatment of cellular functional diseases and the development of drug medicine. This work presented the application potential of liquid metal in microfluidics as a microelectrode for cell manipulation.

II. MATERIALS AND METHODS

A. SAMPLE PREPARATION

Blood samples were obtained from the veins of healthy mice, added with ethylenediamine tetraacetic acid anticoagulant to prevent blood clotting, and stored in a 4 °C sterile environment before the experiment. The liquid metal, which included 67% Ga, 20.5% In, and 12.5% Sn, was used in the experiment as an electrode and stored in NaOH solution to prevent oxidation. Red blood cells were added into the DEP buffer, which contained 8.5% w/w sucrose, 0.3% w/w dextrose, and 20 mg/L $CaCl_2$ and had electrical conductivity and relative permittivity of approximately 10 mS/m and 78, respectively [42], [43]. This configuration allowed the application of the DEP force on red blood cells without burning the electrodes. The experiments were completed within 2 h to maintain cell activity. Prior to the experiments, the channel was rinsed with deionized water and absolute ethanol and treated with 1% BSA to prevent cell adhesion.

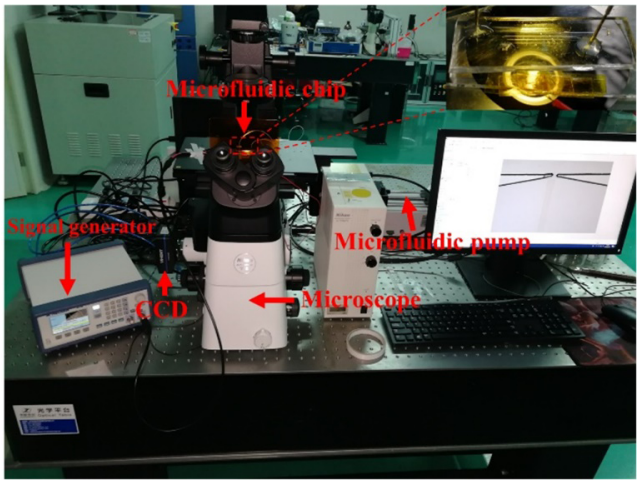

FIGURE 1. Manipulation system consisting of a signal generator, a microscope, a microfluidic pump and a CCD.

B. MANIPULATION SYSTEM

The manipulation system for the measurement and analysis of cell mechanical properties mainly included the following parts (Fig. 1). First, the signal generator was used to generate sinusoidal voltage waveform, and the microfluidic pump was selected to inject cells and liquid metal into the microchannels. Second, a microscope (Nikon) and a CCD camera were used to observe and record cell deformation, respectively. Third, a polydimethylsiloxane (PDMS)-based microfluidic chip was designed and fabricated to perform cell stretching experiments.

The microfluidic chip consisted of a pair of electrodes made of ITO and liquid metal, and two PDMS (Sylgard 184, Dow Corning) microchannels, namely, liquid metal microchannel (LMC) and DEP buffer microchannel (DMC, Fig. 2). Both microchannels had a width of 1000 μm and a length of 3 cm and were separated by a 300 μm-thick PDMS wall. An interconnected microchannel (IMC) was placed in the middle of the two channels to ensure that the electric field intensity formed by the liquid metal is sufficient. Meanwhile, the IMC must be sufficiently narrow to prevent the liquid metal from flowing into the DEP buffer channel. The structure of the right-angled triangle facilitated cell flow toward the ITO electrode to increase the cell capture rate. The thickness of the ITO electrode was 180 nm. The liquid metal and ITO electrodes were located on both sides of the PDMS wall, and the distance between the two electrodes was 40 μm.

The DEP microfluidic chip was fabricated mainly based on soft-lithography and lift-off technologies. The ITO electrode and PDMS microchannels were constructed using soft lithography techniques using the following steps. First, a positive photoresist (RZJ-304) was applied to the ITO conductive

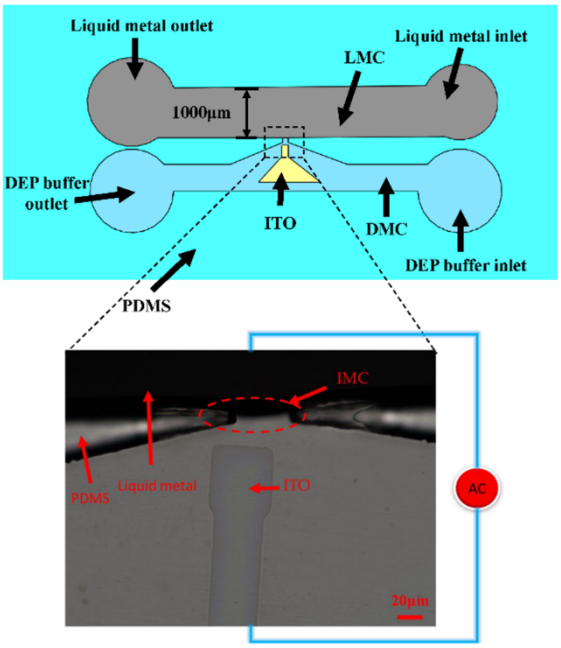

FIGURE 2. Scheme of microfluidic chip. Microfluidic chip consisting of ITO electrode and two microchannels; the scale bar was 20 μm.

glass at a rate of 3500 rpm to produce a 2 μm-thick photoresist layer, which was baked at 100 °C for 3 min and then exposed to 365 nm UV light at an energy density of 12.4 mJ/cm^2 for 2 s. The exposed ITO conductive glass was developed with a developer (RZX-3038) for 1 min and blow dried with nitrogen to fabricate a patterned electrode. Second, a negative photoresist (Microchem Corp su-8 2050) was spin coated on a 4 in Si wafer at 2500 rpm for 30 s to manufacture a film with the thickness of 50 μm. After baking at 65 °C for 2 min and 95 °C for 7 min, the Si wafer was exposed to 365 nm UV light at an energy density of 12.4 mJ cm^{-2} for 10 seconds. The Si wafer was then prebaked with the same parameters and developed using the developer for 1 min. A patterned negative photoresist mold was fabricated. Exactly 30 g of PDMS mixed with curing agent at a ratio of 10:1 by weight was poured onto the mold after being placed in a vacuum oven to remove the bubbles for 0.5 h. After baking at 85 °C for 30 min, the PDMS microchannels were separated from the mold and cut to the appropriate size. Finally, the PDMS microchannels and ITO electrode were placed into the plasma cleaner for 2 min via oxygen plasma treatment and then baked at 95 °C for 10 min to ensure that the bonds were tight, and the liquid metal and DEP buffer did not leak. The inlet and outlet of the chip were connected to a polytetrafluoroethylene tube for sample injection and collection. The liquid metal was injected into the LMC at a rate of 5 μL/min by a syringe pump. The ITO and liquid metal electrodes were connected to the two joints of the signal generator to generate a non-uniform electric field to capture and stretch the cells.

C. THEROTICAL ANASLYSIS

It was assumed that the RBCs stretched by DEP have ellipsoidal structure. The DEP force F_{DEP} can be estimated by the follow equation [44], [6]:

$$F_{DEP} = \pi abc\varepsilon_m Re[f_{CM}]\nabla E_{rms}^2, \tag{1}$$

where f_{CM} denotes the Clausius–Mossotti factor, ε_m denotes the permittivity of the suspending medium, $Re\,[f_{CM}]$ denotes the actual component of the f_{CM}, and ∇E_{rms}^2 denotes the gradient of the square of the applied electric field E. a and b are the major and minor radii of the RBC, which were measured from the experimental images. c denotes the thickness of the RBC, which was assumed as constant (2 μm) because the deformation mainly taken place along the major and minor axes. The effective permittivity of the RBC was estimated with a single-shell structure model, expressed as in (2) [6], as shown at the bottom of this page.

where the subscripts *cyto*, *mem* and *m* represent cytoplasm, membrane and medium, respectively.$\varepsilon^* = \varepsilon - j\sigma/\omega$, where ω denotes angular frequency, ε denotes the dielectric permittivity, $j = \sqrt{-1}$. The electrical conductivity $\rho =$ (a-t) $(b-t)^2/ab^2$, where t denotes the thickness of cell membrane, which was set as 4.5nm in this study. $\varepsilon_{mem} = 4.44$, $\varepsilon_{cyto} = 59$, $\sigma_{mem} = 10^{-6}$S/m, $\sigma_{cyto} = 0.31$S/m [6]. A_i is the depolarization factor which can be given as:

$$A_i = \frac{1-e_i^2}{2e_i^3}\left[log\frac{1-e_i}{1+e_i} - 2e_i\right], i = 1, 2 \tag{3}$$

where $e_1 = \sqrt{1-(\frac{b}{a})^2}$, $e_2 = \sqrt{1-(\frac{b-2t}{a-2t})^2}$. Values of Re($f_{CM}$) for RBCs in this experiments were calculated by MATLAB R2014a (FIG. 3).

The electric field between the liquid metal electrode and the ITO electrode was simulated by the finite element software (COMSOL 5.2a), where the depth of the color represents the strength of the electric field gradient. The 0 point of the abscissa denotes the edge of the ITO electrode, and the 40 μm point indicates the edge of the liquid metal electrode. Fig. 4 shows the schematics and simulation results of the presence or absence of IMC between the liquid metal electrode and the ITO electrode. The electric field was substantially completely shielded without IMC because the relative dielectric constant of PDMS is only 2.76 and the relative dielectric constant of DEP buffer is approximately 78. Due to the presence of IMC, a sufficiently large electric field

$$f_{CM} = \frac{1}{3}\frac{(\varepsilon_{mem}^* - \varepsilon_m^*)\left[\left(\varepsilon_{mem}^* + A_1\left(\varepsilon_{cyto}^* - \varepsilon_{mem}^*\right)\right] + \rho(\varepsilon_{cyto}^* - \varepsilon_{mem}^*)\left[\left(\varepsilon_{mem}^* - A_1\left(\varepsilon_{mem}^* - \varepsilon_m^*\right)\right]\right.\right.}{\left(\varepsilon_m^* + A_1\left(\varepsilon_{mem}^* - \varepsilon_m^*\right)\right)\left[\left(\varepsilon_{mem}^* + A_1\left(\varepsilon_{cyto}^* - \varepsilon_{mem}^*\right)\right]\right. + \rho A_2(1-A_1)(\varepsilon_{cyto}^* - \varepsilon_{mem}^*)\left(\varepsilon_{mem}^* - \varepsilon_m^*\right)}, \tag{2}$$

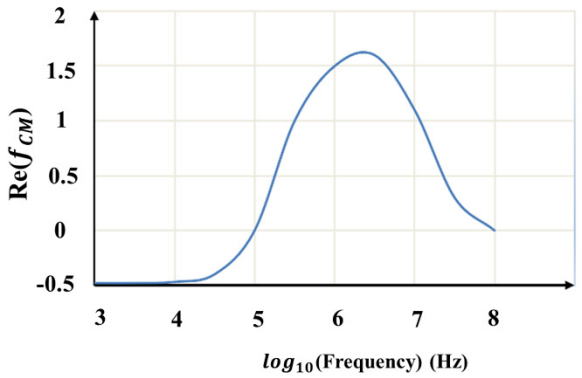

FIGURE 3. Values of $Re[f_{CM}]$ with electrical frequencies between 1 kHz and 100 MHz.

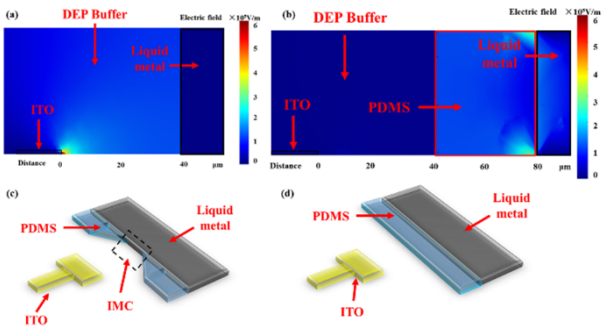

FIGURE 4. Simulation diagram of electric field gradient between liquid metal electrode and ITO electrode. The voltage and frequency were set to 9 Vpp and 1.5 MHz, respectively. (a) With IMC; (b) Without IMC; (c) Schematic diagram containing IMC; (d) Schematic diagram without IMC.

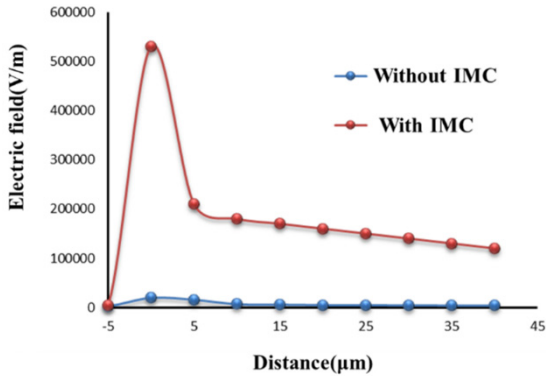

FIGURE 5. Specific numerical variation of the electric field gradient between the liquid metal electrode and the ITO electrode.

gradient was formed between the liquid metal electrode and the ITO electrode when energized. The IMC made it possible to capture and stretch cells with liquid metal electrode in microfluidic chip. It can be seen more intuitively in Fig. 5 that the electric field intensity near the edge of the ITO electrode increased from 1.2×10^4 V/m to 5.4×10^5 V/m. The voltage and frequency were set to 9 Vpp and 1.5 MHz, respectively.

The electric field gradient can be adjusted by changing the voltage. A small electrodes distance leads to a large electric field gradient at the edge of the ITO electrode. A sine wave

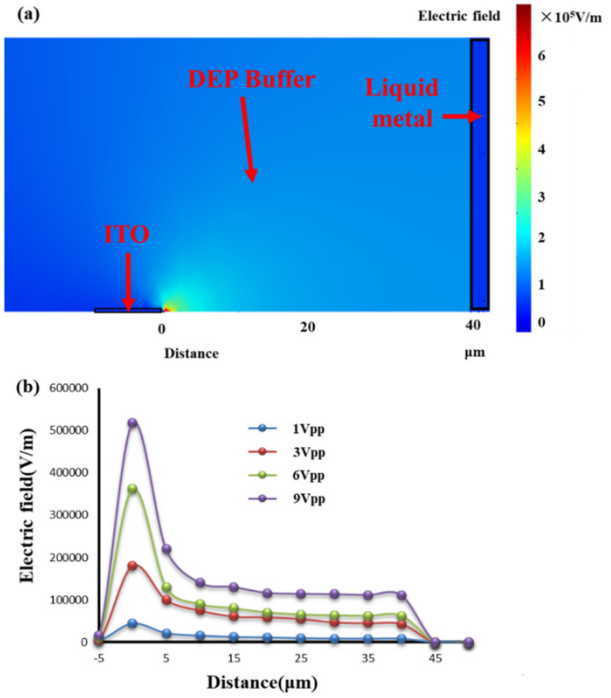

FIGURE 6. Electric field distribution. (a) Simulation of electric field generated by ITO and liquid metal electrodes using finite element software COMSOL; the voltage and frequency were set to 9 Vpp and 1.5 MHz, respectively. (b) Specific numerical variation of electric field gradient between liquid metal and ITO electrodes; the voltages were set to 1, 3, 6, and 9 Vpp.

with 6 Vpp and a frequency of 1.5 MHz can generate a DEP force of 50 pN to stretch the cells when the distance between the two electrodes is 40 μm. Therefore, 8 Vpp is needed to generate the same DEP force when the distance is 60 μm. The 20 μm distance can generate a DEP force of 100 pN. However, the diameter of the red blood cells was $\sim$10 μm. The channel may be clogged when the distance between the liquid metal and ITO electrodes is extremely small. In terms of manufacturing, the precise alignment of the platform is highly required when the distance between the ITO and liquid metal electrodes is small. Hence, the distance between the ITO and liquid metal electrode was set as 40 μm, which allows easy manufacturing and can generate sufficient electric field gradient to stretch the red blood cells (Fig. 6(a)). At this distance, the electric field generated by the electrodes was sufficient to capture and stretch the red blood cells. Fig. 6(b) shows a numerical image of the change in electric field strength from the ITO electrode to the liquid metal electrode. The voltage increased from 1 Vpp to 9 Vpp. The electric field intensity near the edge of the ITO increased from 5×10^4 V/m to 5.3×10^5 V/m. Hence, the electric field intensity increased with the voltage. According to the principles above, cell capturing and stretching are feasible.

The thickness of the ITO electrode was $\sim$180 nm, and that the liquid metal electrode was 50 μm. The significant height difference between the ITO and liquid metal electrodes height allowed the formation of high electric field gradient. A capacitive effect occurs between two liquid metal electrodes which

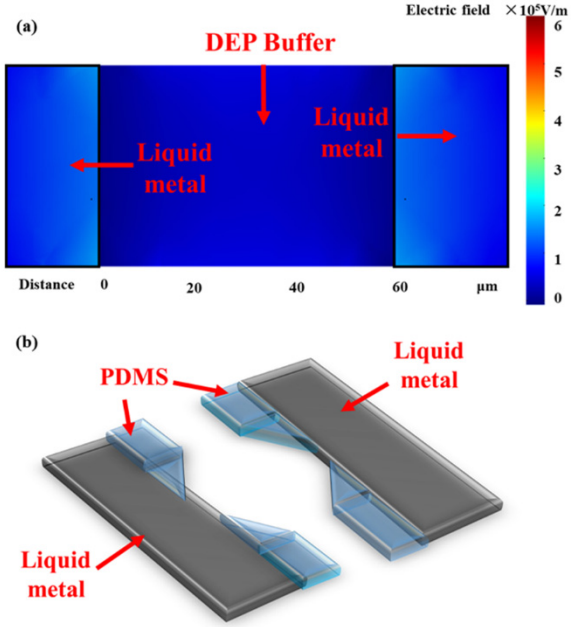

FIGURE 7. (a) Diagram of electric field gradient between pair of liquid metal electrodes. The voltage and frequency were set to 9 Vpp and 1.5 MHz, respectively. (d) Scheme of a pair of liquid metal electrodes.

have the same height. Similar to two conductors that are close together, the two liquid metal electrodes have a layer of non-conductive insulating medium sandwiched between them. This medium will not produce enough electric field gradient to stretch the cells. Figure 7 illustrates that almost no electric field gradient existed between the liquid metal electrodes. Therefore, a pair of electrodes made of liquid metal and ITO was chosen in our experiment.

D. CELL STRETCHING PROTOCOL

A function generator was used to generate sinusoidal voltage signal. Selecting the frequency is crucial because it determines the polarity and the magnitude of the DEP force. A sine wave with a low voltage was applied to the electrodes to initially capture red blood cells, and the voltage was then increased to stretch the cells. A CCD camera was used to observe and record the deformation of the cells, and image processing software was used to process the cell deformation images.

Fig. 8 shows the capture and stretch processes of red blood cells. The red blood cells initially flowed forward along the microchannel when no voltage was applied (Fig. 8 (a)). When the DEP buffer injection was stopped, a sine voltage wave with a frequency of 1.5 MHz and 1 Vpp was applied to the ITO and liquid metal electrodes to capture the red blood cell on the ITO electrode side (Fig. 8 (b)). The cells in other locations cannot be trapped due to insufficient voltage gradient. After the cells were successfully captured, the voltage was increased from 1 Vpp to 10 Vpp on both sides of the electrode by 1 Vpp each time. The cells in our experiment were stretched for 20 s and released for 10 s at each voltage to measure the deformation and recovery properties. Each cell was

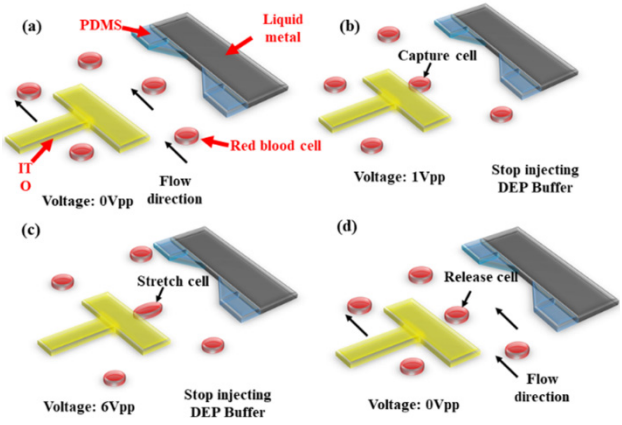

FIGURE 8. Scheme of cell-stretching process. (a) When no voltage was applied, the cells flowed forward along the microchannel; (b) Microfluidic syringe pump was stopped, and a sine wave with 1 Vpp and a frequency of 1.5 MHz were applied to capture the red blood cell; (c) Voltage was increased to stretch the cell; (d) After stretching, the voltage signal was removed and the syringe pump was turned on to wash away the cells.

stretched no more than 10 times, thereby avoiding dynamic fatigue behaviors caused by repeated stretching [6]. Cellular deformation was observed and recorded by microscope and CCD camera (Fig. 8 (c)). When the measurement was completed, the power supplies of the liquid metal and ITO electrodes were turned off (Fig. 8 (d)). The liquid metal can be recycled by syringe pump. DMC and LMC were flushed with absolute ethanol for subsequent use.

III. RESULTS AND DISCUSSION

A. ANALYSIS OF LIQUID METAL CHANNEL WIDTH

The LMC and DMC were interconnected through an IMC. The liquid metal should flow normally while avoiding penetration into the DMC. The LMC was designed as 1000 μm in width and 50 μm in height. The width of the microhole that connects the two microchannels was especially critical. When the width of the IMC was large, the surface tension of the liquid metal was small, and the liquid metal can flow into the DMC from the LMC. When the width of the IMC was $<$50 μm, the chip would become difficult to manufacture, and the intermediate PDMS barrier would weaken the electric field and would require a large voltage to generate the DEP force, which can cause damage to the electrode.

Liquid metal was injected into the microchannel by a microfluidic syringe pump at a flow rate of 5 μL/min. Figure 9(a) shows an image of liquid metal flow at different widths of IMC. The width of the IMC was 60, 70, 80, and 90 μm from left to right. When the width of the IMC was $<$100 μm, the liquid metal flowed forward without penetrating into the DMC. When the width of the IMC was $>$100 μm, a small portion of the liquid metal penetrated into the DMC to affect the cell stretching experiment (Fig. 9 (b)). As the width of the IMC increased, increasing liquid metal permeated into the DMC. The widths of the IMC in Fig. 9 (b) were 100, 150, 200, 250, 300, 350, 400, and 450 μm. Evidently, a large amount of liquid metal began to permeate and formed

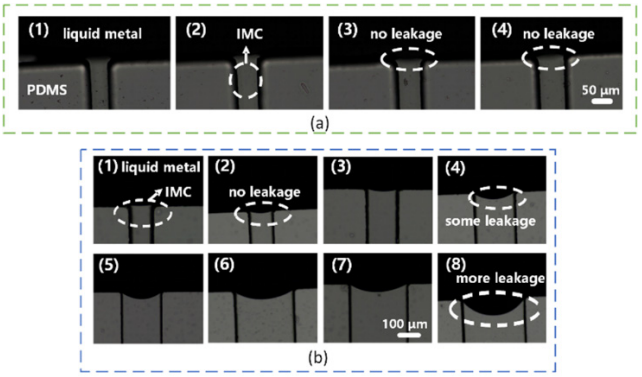

FIGURE 9. Images of liquid metal flows with different IMC widths. (a) From left to right, the widths of the IMC were 60, 70, 80, and 90 μm, and the scale bar is 50 μm. (b) The widths of the IMC were 100, 150, 200, 250, 300, 350, 400, and 450 μm, and the scale bar is 100 μm.

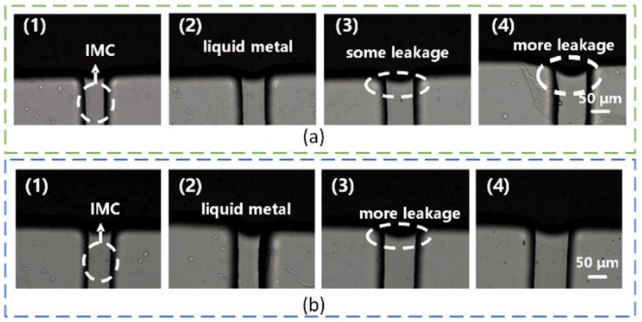

FIGURE 10. Different injection speeds of liquid metal from left to right. The widths of the IMCs were 60, 70, 80, and 90 μm; the scale bar was 50 μm. (a) The injection rate of the liquid metal was 10 μL/min. (b) The injection rate of the liquid metal was 15 μL/min.

an arc shape when the width of the IMC was >200 μm. Hence, the analysis above showed that it was more suitable for experiments when the width of IMC was <100 μm.

B. ANALYSIS OF LIQUID METAL FLOW RATE

The injected speed of the liquid metal into the microfluidic chip also affected the experimental process, which should be analyzed. When the liquid metal was injected at an extremely slow rate, it consumed substantial amount of time to completely fill the LMC with a width of 1000 μm and a length of 3 cm. Conversely, if the liquid metal was injected at an extremely fast rate, the liquid metal would easily penetrate into the DMC from the IMC, thereby also affecting the success of this experiment.

Fig. 9 (a) shows the flow of liquid metal in the microchannel when the injection rate of liquid metal was 5 μL/min, almost no excess liquid metal was permeated. The injection rate of liquid metal increased, and when the injection rate of liquid metal reached 10 μL/min, a small portion of the liquid metal in the 60—90 μm width IMC began to penetrate (Fig. 10 (a)). In another batch of microfluidic chips, the injection rate of liquid metal continuously increased to 15 μL/min, and the liquid metal penetrated, thereby affecting our experiment (Fig. 10 (b)). When the injection rate

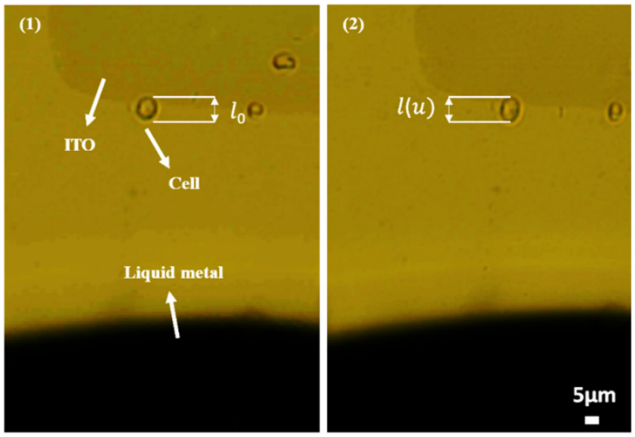

FIGURE 11. When the electrodes are not energized, the length of the red blood cell is denoted as l_0. When a sine wave with 3 Vpp and 1.5 MHz is applied to the liquid metal electrode and ITO electrodes, the length of the cell is denoted as l (u); the scale bar is 5 μm.

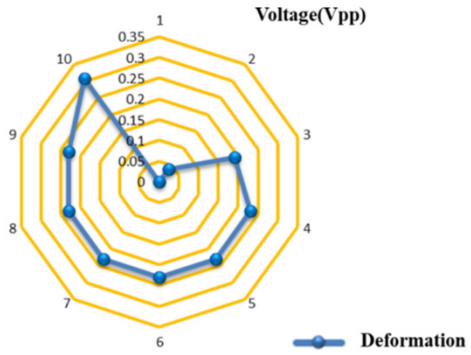

FIGURE 12. Voltage between ITO and liquid metal electrodes increased from 1 Vpp to 10 Vpp, and the degree of deformation of the cell increased from 0 to 0.31.

of the liquid metal was slow, although the liquid metal did not permeate, the time required to fill the LMC was long. In summary, an injection rate of 5 μL/min was be the most suitable speed in this experiment.

C. CELL DEFORMATION

Cell deformation was observed and recorded by a microscope and CCD camera, and the degree of cell deformation was defined as D by the following formula:

$$D(u) = \frac{l(u) - l_0}{l_0}, \tag{4}$$

where u denotes the peak-to-peak value of the magnitude of the voltage, l_0 denotes the original length of the cell, and $l(u)$ denotes the length of the cell after deformation at the voltage of u (Fig. 11).

A sine wave with 1 Vpp and a frequency of 1.5 MHz was applied to the ITO and the liquid metal to capture cells on the ITO side. The relationship between the voltage and cell deformation was analyzed by an image processing software (Fig. 12). The length at which the cell was captured at the edge of the ITO electrode in Fig. 7 was used as the initial length. When the voltage was increased

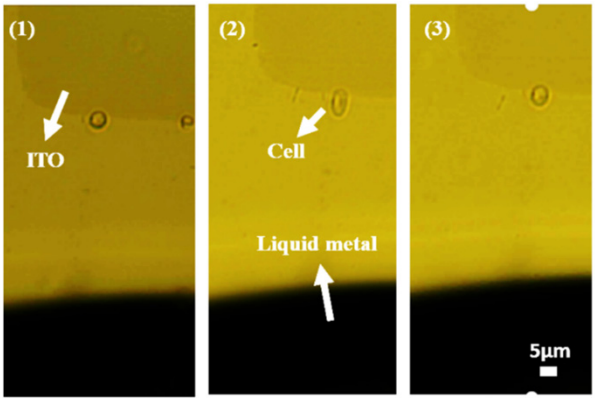

FIGURE 13. After applying a 10 Vpp sine wave to liquid metal and ITO electrodes to stretch the cell for 20 s, the cell did not return to its original shape. The scale bar was 5 μm.

from 1 Vpp to 2 Vpp, the degree of deformation of the cell was small, thereby increasing only from 0 to 0.05. When the voltage was >2 Vpp, the degree of cell deformation increased almost linearly with the increase in voltage. When the voltage was >4 Vpp, the degree of cell deformation was >0.19. As the voltage increased to 9 Vpp, the degree of cell deformation was essentially ∼0.23. However, in our experiments, a phenomenon was found when the voltage applied to the electrode was >10 Vpp, that is, after the cell was stretched for 20 s, the cells cannot return to their original shape even if the power was turned off. When the voltage was extremely high, and the cells were stretched for a long time, the inner structure of the cells may be destroyed and cannot be restored to their original shape (Fig. 13). For example, the initial length of one target red blood cell was 5 μm. However, after applying a 10 Vpp sine wave on the electrode for 20 s, the cell can only recover to approximately 6 μm. Therefore, with the increase of the voltage, the degree of cell deformation cell also increased when the cell tissue structure was not destroyed. When the deformation of the cell reached its maximum, the voltage continued to increase from 5 Vpp to 9 Vpp, and the cell did not undergo a greater degree of deformation. The voltage continued to increase to 10 Vpp, the deformation of the cell increased suddenly, the structure of the cell would be destroyed, and the cell cannot return to its original length.

The degree of cell deformation can be expressed in another quantitative approach, that is, by the value of the positive DEP force applied on the cells (Table 1). Table 1 presents the data acquired at 20 s. When the cell suffered a positive DEP force of <10 pN, the red blood cell did not undergo significant deformation. As the DEP force continued to increase, the deformation of the red blood cell became large until the positive DEP force reached 25 pN. The deformation of the cell variable reached the maximum value of 0.23. Subsequently, the DEP force continued to increase, but the deformation of the cell slightly changed. However, after the cell received a positive DEP force greater than 100 pN, cell deformation became large again, and this deformation

TABLE 1. DEP force applied to RBCs.

Voltage (Vpp)	Deformation $D(u)$	DEP Force (pN)
1	0	0.7
2	0.05	2.5
3	0.038	8.9
4	0.192	13.3
5	0.231	25.2
6	0.231	38.5
7	0.231	50.4
8	0.231	62.2
9	0.231	83.0
10	0.308	103.7

TABLE 2. Force applied to the cells.

Paper	Method	Force (pN)	Strain
[40]	OT	100	0.37
[41]	OT	100	0.41
[42]	DEP	100	0.33
Our paper	DEP	100	0.31

was irreversible. The cell structure may be destroyed after being subjected to a particularly large DEP force.

D. RESULTS ANALYSIS

To verify the accuracy of our experimental data, we also reviewed a series of related works on the basis of optical tweezers (OT) and DEP [40], [41] (Table 2). For example, in an article [40], the axial diameter of the red blood cell increased from 8 μm to 15 μm when suffering from the stretching force of ∼200 pN. The axial diameter of the cell increased by 37% at approximately 100 pN. The RBC was regarded with a single-shell structure in this study as the cell consists of membrane and cytoplasm, which was simpler than that in Suresh [39] 's work. Different structure models will lead to differences in the measurement results. Under different cell models and methods, the experimental results will have subtle difference within an acceptable range.

IV. CONCLUSION

In this paper, Galinstan liquid metal was first introduced into the microfluidic chip as microelectrode to form a nonuniform electric field. The detailed applicable conditions of the liquid metal electrode were analyzed, including IMC width and liquid metal injection rate. A cell manipulation system was built to measure and analyze the mechanical properties of cells. A novel microfluidic chip integrated with liquid metal electrode was designed and fabricated. The use of liquid metal electrode not only enabled the rapid and accurate measurement of the mechanical properties of cells but also provides several unique advantages including easy manufacturing, low cost, hard to be broken down by high voltage, and reusability. Meanwhile, we analyzed the effect of the voltage applied to the electrodes on cell deformation. A series

of experiments was performed to stretch the mice red blood cells, which showed that the deformation of the cell increased with the increase in voltage until the maximum was reached. This work not only demonstrated the potential of using liquid metal as an electrode in microfluidic chip but also laid the foundation for cell and microparticle manipulation (e.g., rotation and separation) in microfluidic systems by liquid metal electrode. The physiological properties of the cell can also be explained by analyzing the mechanical properties of the cell, which may contribute to the treatment of cellular functional diseases and medicine development.

REFERENCES

[1] M. M. Brandžo, A. Fontes, M. L. Barjas-Castro, L. C. Barbosa, F. F. Costa, C. L. Cesar, and S. T. O. Saad, "Optical tweezers for measuring red blood cell elasticity: Application to the study of drug response in sickle cell disease," *Eur. J. Haematol.*, vol. 70, no. 4, pp. 207–211, 2003.

[2] X. Mao and T. J. Huang, "Exploiting mechanical biomarkers in microfluidics," *Lab Chip*, vol. 12, no. 20, pp. 4006–4009, 2012.

[3] S. E. Cross, Y.-S. Jin, J. Rao, and J. K. Gimzewski, "Nanomechanical analysis of cells from cancer patients," *Nature Nanotechnol.*, vol. 2, no. 12, p. 780, 2007.

[4] L. Huang, P. Zhao, and W. Wang, "3D cell electrorotation and imaging for measuring multiple cellular biophysical properties," *Lab Chip*, vol. 18, no. 16, pp. 2359–2368, 2018.

[5] T. Luo, L. Fan, Y. Zeng, Y. Liu, S. Chen, Q. Tan, R. H. W. Lam, and D. Sun, "A simplified sheathless cell separation approach using combined gravitational-sedimentation-based prefocusing and dielectrophoretic separation," *Lab Chip*, vol. 18, no. 11, pp. 1521–1532, 2018.

[6] Y.-H. Qiang, J. Liu, and E. Du, "Dynamic fatigue measurement of human erythrocytes using dielectrophoresis," *Acta Biomaterialia*, vol. 57, pp. 352–362, Jul. 2017.

[7] X. Zhang, H. K. Chu, Y. Zhang, G. Bai, K. Wang, Q. Tan, and D. Sun, "Rapid characterization of the biomechanical properties of drug-treated cells in a microfluidic device," *J. Micromech. Microeng.*, vol. 25, no. 10, 2015, Art. no. 105004.

[8] G. Bai, Y. Li, H. K. Chu, K. Wang, Q. Tan, J. Xiong, and D. Sun, "Characterization of biomechanical properties of cells through dielectrophoresis-based cell stretching and actin cytoskeleton modeling," *Biomed. Eng. Online*, vol. 16, no. 1, 2017, Art. no. 41.

[9] C. Wu, X. Zhu, T. Man, P.-S. Chung, M. A. Teitell, and P.-Y. Chiou, "Lift-off cell lithography for cell patterning with clean background," *Lab Chip*, vol. 18, no. 20, pp. 3074–3078, 2018.

[10] K. Wang, J. Cheng, S. H. Cheng, and D. Sun, "Probing cell biophysical behavior based on actin cytoskeleton modeling and stretching manipulation with optical tweezers," *Appl. Phys. Lett.*, vol. 103, no. 8, 2013, Art. no. 083706.

[11] H.-D. Polaschegg, "Red blood cell damage from extracorporeal circulation in hemodialysis," *Seminars Dialysis*, vol. 22, no. 5, pp. 524–531, 2009.

[12] Y. M. Efremov, M. E. Lomakina, and D. V. Bagrov, "Mechanical properties of fibroblasts depend on level of cancer transformation," *Biochim. Biophys. Acta*, vol. 1843, no. 5, pp. 1013–1019, May 2014.

[13] D. Discher, C. Dong, J. J. Fredberg, F. Guilak, D. Ingber, P. Janmey, R. D. Kamm, G. W. Schmid-Schönbein, and S. Weinbaum, "Biomechanics: Cell research and applications for the next decade," *Ann. Biomed. Eng.*, vol. 37, no. 5, p. 847, 2009.

[14] S. Suresh, J. Spatz, J. P. Mills, A. Micoulet, M. Dao, C. T. Lim, M. Beil, and T. Seufferlein, "Connections between single-cell biomechanics and human disease states: Gastrointestinal cancer and malaria," *Acta biomaterialia*, vol. 1, no. 1, pp. 15–30, 2005.

[15] S. Suresh, "Biomechanics and biophysics of cancer cells," *Acta Mater.*, vol. 55, no. 12, pp. 3989–4014, 2007.

[16] G. A. Barabino, M. O. Platt, and D. K. Kaul, "Sickle cell biomechanics," *Annu. Rev. Biomed. Eng.*, vol. 12, pp. 345–367, Aug. 2010.

[17] E. A. Evans, R. Waugh, and L. Melnik, "Elastic area compressibility modulus of red cell membrane," *Biophys. J.*, vol. 16, no. 6, pp. 585–595, 1976.

[18] E. J. Koay, A. C. Shieh, and K. A. Athanasiou, "Creep indentation of single cells," *J. biomechanical Eng.*, vol. 125, no. 3, pp. 334–341, 2003.

[19] S. Warnat, H. King, C. Forbrigger, and T. Hubbard, "PolyMUMPs MEMS device to measure mechanical stiffness of single cells in aqueous media," *J. Micromech. Microeng.*, vol. 25, no. 2, 2015, Art. no. 025011.

[20] L. Xiao, M. Tang, Q. Li, and A. Zhou, "Non-invasive detection of biomechanical and biochemical responses of human lung cells to short time chemotherapy exposure using AFM and confocal Raman spectroscopy," *Anal. Methods*, vol. 5, no. 4, pp. 874–879, 2013.

[21] H. W. Hou, Q. S. Li, G. Y. H. Lee, A. P. Kumar, C. N. Ong, and C. T. Lim, "Deformability study of breast cancer cells using microfluidics," *Biomed. Microdevices*, vol. 11, no. 3, pp. 557–564, 2009.

[22] G. Guan, P. C. Y. Chen, W. K. Peng, A. A. Bhagat, C. J. Ong, and J. Han, "Real-time control of a microfluidic channel for size-independent deformability cytometry," *J. Micromech. Microeng.*, vol. 22, no. 10, 2012, Art. no. 105037.

[23] H. H. See, S. C. B. Herath, Y. Du, Y. Du, H. Asada, and P. C. Y. Chen, "Localized manipulation of magnetic particles in an ensemble," *IEEE Access*, vol. 6, pp. 24075–24088, 2018.

[24] Y. Tan, C.-W. Kong, S. Chen, S. H. Cheng, R. A. Li, and D. Sun, "Probing the mechanobiological properties of human embryonic stem cells in cardiac differentiation by optical tweezers," *J. Biomech.*, vol. 45, no. 1, pp. 123–128, 2012.

[25] Y. Xu, H. Yang, J. Li, J. Liu, and N. Xiong, "An effective dictionary learning algorithm based on FMRI data for mobile medical disease analysis," *IEEE Access*, vol. 7, pp. 3958–3966, 2019.

[26] Q. S. Li, G. Y. H. Lee, C. N. Ong, and C. T. Lim, "AFM indentation study of breast cancer cells," *Biochem. Biophys. Res. Commun.*, vol. 374, no. 4, pp. 609–613, Oct. 2008.

[27] I. Doh and Y. H. Cho, "A continuous cell separation chip using hydrodynamic dielectrophoresis (DEP) process," *Sens. Actuators A, Phys.*, vol. 121, no. 1, pp. 59–65, 2005.

[28] H. S. Moon, K. Kwon, S.-L. Kim, H. Han, J. Sohn, S. Lee, and H.-I. Jung, "Continuous separation of breast cancer cells from blood samples using multi-orifice flow fractionation (MOFF) and dielectrophoresis (DEP)," *Lab Chip*, vol. 11, no. 6, pp. 1118–1125, 2011.

[29] T. C. Shih, K. H. Chu, and C. H. Liu, "A programmable biochip for the applications of trapping and adaptive multisorting using dielectrophoresis array," *J. Microelectromech. Syst.*, vol. 16, no. 4, pp. 816–825, Aug. 2007.

[30] D. S. Gray, J. L. Tan, J. Voldman, and C. S. Chen, "Dielectrophoretic registration of living cells to a microelectrode array," *Biosensors Bioelectron.*, vol. 19, no. 12, pp. 1765–1774, 2004.

[31] M. M. Keane, G. A. Lowrey, S. A. Ettenberg, M. A. Dayton, and S. Lipkowitz, "The protein tyrosine phosphatase DEP-1 is induced during differentiation and inhibits growth of breast cancer cells," *Cancer Res.*, vol. 56, no. 18, pp. 4236–4243, 1996.

[32] S. C. Tan, B. Yuan, and J. Liu, "Electrical method to control the running direction and speed of self-powered tiny liquid metal motors," *Proc. Roy. Soc. A, Math., Phys. Eng. Sci.*, vol. 471, no. 2183, Nov. 2015, Art. no. 20150297.

[33] M. Gao and L. Gui, "A handy liquid metal based electroosmotic flow pump," *Lab Chip*, vol. 14, no. 11, pp. 1866–1872, 2014.

[34] J. Jeon, J.-B. Lee, and S. K. Chung, "On-demand magnetic manipulation of liquid metal in microfluidic channels for electrical switching applications," *Lab Chip*, vol. 17, pp. 128–133, Oct. 2016.

[35] J.-H. So and M.-D. Dickey, "Inherently aligned microfluidic electrodes composed of liquid metal," *Lab Chip*, vol. 11, no. 5, p. 905, 2011.

[36] L. Tian, L. Zhang, M. Gao, Z. Deng, and L. Gui, "A handy liquid metal based non-invasive electrophoretic particle microtrap," *Micromachines*, vol. 9, no. 5, p. 221, May 2018.

[37] Y. T. Chow, T. Man, G. F. Acosta-Vélez, X. Zhu, X. Wen, P.-S. Chung, T. L. Liu, B. M. Wu, and P.-Y. Chiou, "Liquid metal-based multifunctional micropipette for 4D single cell manipulation," *Adv. Sci.*, vol. 5, no. 7, Jul. 2018, Art. no. 1700711.

[38] M. Dao, C. T. Lim, and S. Suresh, "Mechanics of the human red blood cell deformed by optical tweezers," *J. Mech. Phys. Solids*, vol. 51, nos. 11–12, pp. 2259–2280, 2003.

[39] J. P. Mills, L. Qie, M. Dao, C. T. Lim, and S. Suresh, "Nonlinear elastic and viscoelastic deformation of the human red blood cell with optical tweezers," *Mech. Chem. Biosyst.*, vol. 1, no. 3, pp. 169–180, Sep. 2004.

[40] D. A. Fedosov, B. Caswell, and G. E. Karniadakis, "A multiscale red blood cell model with accurate mechanics, rheology, and dynamics," *Biophys. J.*, vol. 98, no. 10, pp. 2215–2225, May 2010.

[41] E. Du, M. Dao, and S. Suresh, "Quantitative biomechanics of healthy and diseased human red blood cells using dielectrophoresis in a microfluidic system," *Extreme Mech. Lett.*, vol. 1, pp. 35–41, Dec. 2014.
[42] S. V. Puttaswamy, S. Sivashankar, R. J. Chen, C. K. Chin, H. Y. Chang, and C. H. Liu, "Enhanced cell viability and cell adhesion using low conductivity medium for negative dielectrophoretic cell patterning," *Biotechnol. J.*, vol. 5, no. 10, pp. 1005–1015, Oct. 2010.
[43] H. K. Chu, Z. Huan, and J. K. Mills, "Three-dimensional cell manipulation and patterning using dielectrophoresis via a multi-layer scaffold structure," *Lab Chip*, vol. 15, no. 3, pp. 920–930, Feb. 2015.
[44] J. E. Gordon, Z. Gagnon, and H.-C. Chang, "Dielectrophoretic discrimination of bovine red blood cell starvation age by buffer selection and membrane cross-linking," *Biomicrofluidics*, vol. 1, no. 4, Nov. 2007, Art. no. 044102.

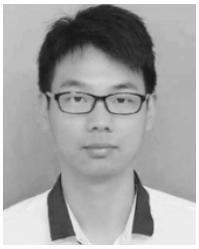

BOTAO ZHU received the B.S. degree from the Department of Automation, Hubei University of Automotive Technology, in 2017. He is currently pursuing the master's degree with the Soochow University. Since 2017, he has been a Research Assistant with the Robotics and Microsystems Center, Soochow University. Since 2017, he has also been involved in microfluidic chips, micro robots, cell mechanism, and liquid metal.

YIFAN CAI received the B.S. degree in mechanical engineering from the Yancheng Institute of Technology. He is currently pursuing the master's degree with Soochow University. Since 2018, he has been a Research Assistant with the Robotics and Microsystems Center, Soochow University. Since 2018, he has also been involved in the microfluidic chips and liquid metal control.

ZHENGTIAN WU received the Ph.D. degree in operations research from the University of Science and Technology of China and the Ph.D. degree from the City University of Hong Kong, in 2014.

From September 2018 to September 2019, he was a Visiting Scholar with the Department of Mechanical Engineering, Politecnico di Milano, Milan, Italy. He is currently an Associate Professor with the Suzhou University of Science and Technology, Suzhou, China. His research interests include neural computation, neural networks, mixed integer programming, approximation algorithm, and distributed computation. He is also a member in Suzhou Key Laboratory for Big Data and Information Service, Suzhou.

FUZHOU NIU received the B.S. degree from the Department of Precision Machinery and Instrumentation, University of Science and Technology of China, Hefei, Anhui, China, in 2010, the Ph.D. degrees in robotics and biomedical engineering from the University of Science and Technology of China, in 2017, and the Ph.D. degree from the City University of Hong Kong, Hong Kong, 2018. He joined the Suzhou University of Science and Technology, in 2018. He is currently an Assistant Researcher with the Department of Mechanical and Electronic Engineering, School of Mechanical Engineering, Suzhou University of Science and Technology, Suzhou, China. His research interests include micro/nano-manipulation, microrobot systems, and bio/micro-robotic applications.

HAO YANG received the B.E. degree in automatic control from the University of Science and Technology of China, Hefei, China, in 2010, the Ph.D. degree in robotics and biomedical engineering from the University of Science and Technology of China, and the Ph.D. degree from the City University of Hong Kong, Hong Kong, in 2015. From 2015 to 2016, he was a Postdoctoral Researcher with the Department of Mechanical and Biomedical Engineering, City University of Hong Kong. He is currently an Associate Professor with the Robotics and Microsystems Center, College of Mechanical and Electrical Engineering, Soochow University, Suzhou, China. His current research interests include robot-aided biomedical systems, cell mechanism, micro/nano manipulation, and micro-robotic applications.